Evaluation of radiometric measurements from the NASA Multiangle Imaging Spectroradiometer (MISR): Two- and three-dimensional radiative transfer modeling of an inhomogeneous stratocumulus cloud deck

Roger Marchand and Thomas Ackerman
Pacific Northwest National Laboratory, Richland, Washington, USA

Received 29 February 2004; revised 13 May 2004; accepted 9 June 2004; published 29 September 2004.

[1] In December 1999, NASA launched the Terra satellite. This platform carries five instruments that measure important properties of the Earth climate system. One of these instruments is the Multiangle Imaging Spectroradiometer, or MISR. This instrument measures light reflected from the Earth at a spatial resolution of 275–1100 m, at four wavelengths (446, 558, 672, and 866 nm), and at nine different viewing angles that vary from +70 to −70 degrees along the direction of flight [*Diner et al.*, 2002]. These multiangle data have the potential to provide information on aerosols, surface, and cloud characteristics that compliments traditional single-view-direction satellite measurements. Before this potential can be realized, the accuracy of the satellite radiance measurements must be carefully assessed, and the implications of the radiometric accuracy on remote-sensing algorithms must be evaluated. In this article, we compare MISR multiangle measurements against two-dimensional (2-D) and 3-D radiative transfer calculations from an inhomogeneous cloud scene. Inputs to the radiative transfer code are based entirely on independently gathered data (ground-based radar, lidar, microwave radiometer, in situ aircraft data, etc.). The 2-D radiative transfer calculations compare favorably near nadir and in most of the forward scattering directions, but differ by as much as 10% in the backscattering directions. Using 3-D radiative transfer modeling, we show that this difference is due to the 3-D structure of the cloud deck, including variations in the cloud top height on scales less than 275 m, which are not resolved in the 2-D simulations. Comparison of the 2-D calculations to the MISR measurements, after accounting for the 3-D structure, show residual differences that are less than 4% at all angles at the MISR blue and green wavelengths. The comparison also reveals that the MISR measurements at the red and near-infrared wavelengths are too bright relative to measurements in the blue and green bands. On the basis of the results of this study, along with results from five other comparisons, the MISR calibration is being adjusted to reduce the red and near-infrared radiances. *INDEX TERMS:* 0360 Atmospheric Composition and Structure: Transmission and scattering of radiation; 3359 Meteorology and Atmospheric Dynamics: Radiative processes; 3360 Meteorology and Atmospheric Dynamics: Remote sensing; *KEYWORDS:* 3-D radiative transfer, satellite remote sensing, satellite calibration

Citation: Marchand, R., and T. Ackerman (2004), Evaluation of radiometric measurements from the NASA Multiangle Imaging Spectroradiometer (MISR): Two- and three-dimensional radiative transfer modeling of an inhomogeneous stratocumulus cloud deck, *J. Geophys. Res.*, *109*, D18208, doi:10.1029/2004JD004710.

1. Introduction

[2] On 3 March 2000, Terra passed over the U.S. Department of Energy Atmospheric Radiation Measurement (ARM) Program Southern Great Plains (SGP) site in Oklahoma. At this site, the ARM program operates an array of ground-based cloud remote-sensing equipment, including a millimeter-wavelength cloud radar, a passive microwave radiometer, broadband solar radiometers, and several lidars. At the time of the satellite overpass, the ARM program was conducting an experiment to measure cloud absorption. As part of this experiment, in situ measurements of cloud microphysics were made using a Forward Spectral Scattering Probe (FSSP) aboard the University of North Dakota citation aircraft.

[3] In this article, we show the results of two-dimensional (2-D) radiative transfer calculations (or simulations) based on the time series data measured by the ground-based instruments at the ARM SGP site. We compare these

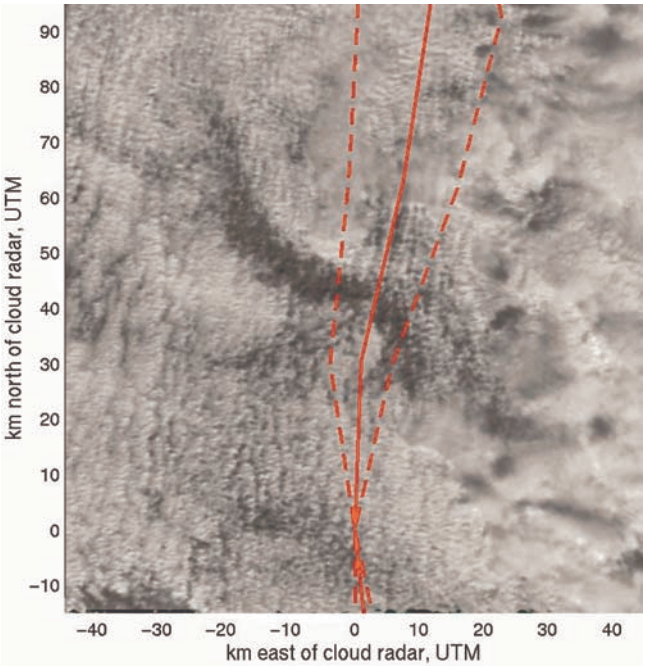

Figure 1. MISR nadir view at 866 nm on a Universal Transverse Mercator (UTM) projection. The solid line shows the best estimate for the cloud advection path over the ARM site. Dashed lines show 1 standard deviation in wind direction. Wind direction and speed estimates were obtained from a 915 MHz wind-profiling radar using 1-hour (consensus) averaging.

simulations with the MISR radiance measurements along an estimate for the cloud advection path. We find that the 2-D calculations (based solely on independently gathered data) reproduce the MISR radiances in the nadir and most of the forward scattering directions. However, in order to explain the observed radiances in the backscattering directions, 3-D calculations with high spatial resolution (greater than 275 m) are required.

[4] A large number of articles have been published, both theoretical and observational in nature, that demonstrate the importance of horizontal photon transport and variations in cloud top height on scattered visible reflectance [e.g., *Loeb and Davies*, 1996; *Davis et al.*, 1997; *Zuidema and Evans*, 1998; *Varnai and Davies*, 1999; *Varnai*, 2000; *Varnai and Marshak*, 2003; *Di Giuseppe and Tompkins*, 2003]. Three-dimensional cloud heterogeneity alters visible reflectance by both smoothing the reflectance field through radiative diffusion and sharpening (or roughing) the brightness variations through illumination of cloud boundaries facing the Sun or generating shadows. These changes in reflectance can cause significant problems for satellite-based retrievals that rely on 1-D radiative transfer theory [*Chambers et al.*, 2001; *Iwabuchi and Hayasaka*, 2002; *Varnai and Marshak*, 2001, 2002].

[5] To account for high-resolution 3-D effects in our 2-D simulations, we use data from an airborne version of the MISR instrument, called AirMISR. The AirMISR measurements are made at the same wavelengths (or bands) and at approximately the same view angles as the MISR measurements, but at a much higher spatial resolution. In section 2 we present our baseline 2-D calculations and in section 3 we describe a novel approach to construct a 3-D cloud field from the AirMISR measurements and estimate the influence of 3-D scattering (including cloud top height structure) that is not included in the initial 2-D simulations. In sections 4 and 5, we examine the 3-D scattering effects in the context of previous studies, as well as the implications for MISR radiometric calibration.

[6] In regards to MISR calibration, comparison of the 2-D simulations to the MISR measurements (after adjusting for the influence of the 3-D structure) shows residual differences that are less than 4% at all angles in the MISR blue and green bands. The comparison also reveals that the MISR measurements in the red and near-infrared bands are too bright relative to measurements in the blue and green bands. On the basis of the results of this study, along with results from five other comparisons (similar in many ways to this study but conducted over clear sky desert playas that are darker than the cloud scene examined here), the MISR calibration is being adjusted to reduce the red and near-infrared radiances. (Results from one of the five experiments mentioned above have been published by *Bruegge et al.* [2002] and *Abdou et al.* [2002].)

2. Two-Dimensional Simulations

[7] Inputs for the 2-D radiative transfer simulations come from a combination of ground-based and aircraft-based measurements. Cloud boundaries from radar and lidar [*Clothiaux et al.*, 2000], and cloud liquid water path retrieved from passive microwave measurements [*Marchand et al.*, 2003] are used as inputs in the radiative transfer calculations. These data are gathered as a time series, which is converted into an equivalent 2-D spatial representation using the average in cloud horizontal wind speed as measured by a 915 MHz wind profiler. The time series data were collected every 20 s and the wind speed was approximately 13 m/s, yielding a horizontal resolution of 260 m.

[8] A constant vertical profile of cloud particle size is used in the simulations. This profile was obtained from coincident in situ FSSP measurements from the citation aircraft, which made numerous descents and ascents through the stratocumulus cloud over the ARM SGP site. The FSSP measurements were corrected for probe-dependent and distribution-dependent optical coincidence effects, Mie curve adjustment, time response, and laser beam inhomogeneity (Private communication, M. Poellet, University of North Dakota). The final results are expected to be accurate to approximately 15% in cloud drop radius and 34% in liquid water content (LWC) [*Baumgardner*, 1983]. These data have been used successfully in several previously published papers, including papers by *Dong et al.* [2002], *Min et al.* [2003], and *Ackerman et al.* [2003]. The FSSP data show the particle effective radius slightly increasing from about 6 μm at cloud base to near 7 μm at cloud top, on average.

[9] The stratocumulus cloud on this day provided almost completely overcast conditions. Figure 1 shows the MISR nadir view image of the cloud field at 866 nm (near-infrared band). Superimposed on this image are three lines. The solid line represents the path of clouds that are most likely to have advected over the ARM SGP site based on radar wind-

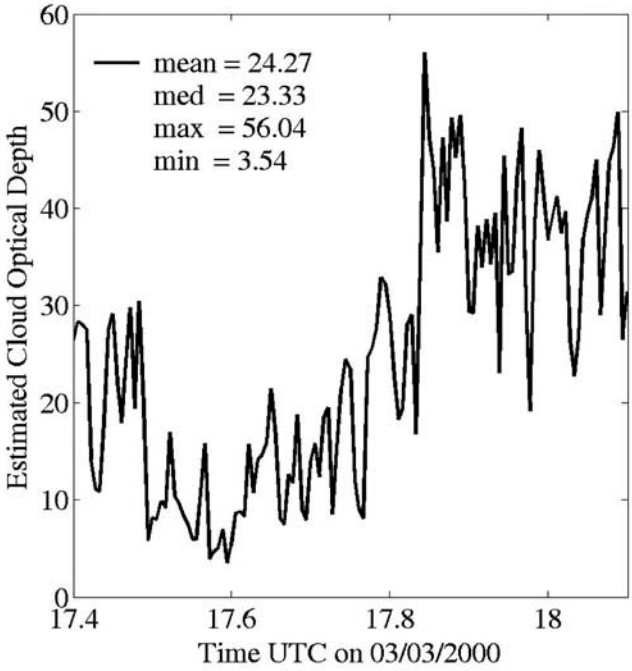

Figure 2. Estimate of cloud optical depth obtained from ARM microwave and broadband radiometer measurements.

profiler measurements. The two dashed lines represent the possible spread in advection path based on a 1 standard deviation change in the average wind direction measurement. The ARM SGP site is located near the bottom of the figure at the intersection of the lines. Figure 2 shows an estimate of the cloud visible optical depth for that portion of the cloud field that passed directly over the ARM SGP site. This estimate is based primarily on the time series retrieval of cloud liquid water path from the microwave radiometer (but with an additional constraint from the measured surface broadband solar flux that will be described momentarily). Figure 2 shows that this cloud was reasonably optically thick on average, with a mean optical depth greater than 24, but with considerable variability. We note the observed variability is much larger than one would obtain from noise in the radiometer measurement.

[10] The radiative transfer calculations were performed using the Spherical Harmonics Discrete Ordinance Method (SHDOM) [*Evans*, 1998]. In the SHDOM code, the cloud droplet phase functions are computed with Mie theory, and delta-M scaling is used in the calculations. Absorption by atmospheric gasses is included using the correlated k technique for both broadband and narrowband calculations. Molecular Rayleigh scattering is included. Atmospheric state variables (pressure, temperature, and humidity with altitude) were obtained from radiosondes, and column ozone was determined from Langley analysis of Sun photometer data gathered during a clear-sky period 5 days prior to the MISR overpass. Molecular scattering is important in the MISR blue band, and ozone absorption is important in the green and red bands at the 5% and 2% level. We ran the calculations using a minimum of 16×32 discrete ordinates and with an initial grid resolution of approximately 260 m in the horizontal and 100 m in the vertical. The SHDOM codes include an adaptive grid splitting routine in which we set the splitting accuracy to 0.01 or better in all calculations. On the basis of our own sensitivity test (the results of which are consistent with those published by *Evans* [1998]) we found the calculations to be accurate at the 1–2% level or better for these parameters.

[11] The SHDOM code permits the surface reflection to be specified via a Lambertian or a Rahman, Pinty, and Verstraete (RPV) model [*Rahman et al.*, 1993]. Because of the nearly complete overcast sky and cloud optical thickness, the inclusion of non-Lambertian surface conditions proved unnecessary. We examined using an RPV surface model in our simulations (with parameters appropriate for grasslands) and found the difference between that and a Lambertian model to be very small. The spectral surface albedo at the SGP site was measured using an Analog Spectral Devices (ASD) spectrometer. The average measured albedo at the MISR wavelengths of 446, 558, 672, and 866 nm was found to be 0.034, 0.075, 0.067, and 0.34 respectively. *Michalsky et al.* [2003] published a paper discussing surface albedo variability near the SGP site during this experiment. Except at 866 nm, where the surface is relatively bright, uncertainty in the radiance calculations due to uncertainty in the surface albedo is smaller than that due to uncertainty in the cloud properties.

[12] Unfortunately, the uncertainty in the 2-D radiance simulations due to uncertainty in the particle effective radius (from in situ probes) and cloud liquid water path (estimated from ARM microwave radiometer data) is undesirably large, exceeding 15%. To reduce this uncertainty, we further constrained the simulations to match the measured solar broadband surface flux, shown in Figure 3. The broadband surface flux measurement is accurate to approximately 10 W/m^2 and the three simulations in Figure 3 span this

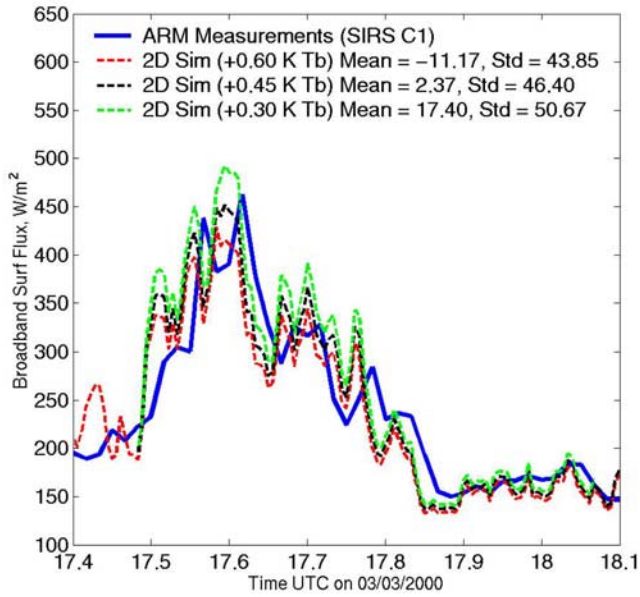

Figure 3. Comparison of simulated and measured broadband surface fluxes. In each simulation a small amount of extra liquid water has been added to the nominal microwave radiometer retrieval, expressed here as an equivalent increase in the 31.4 GHz brightness temperature.

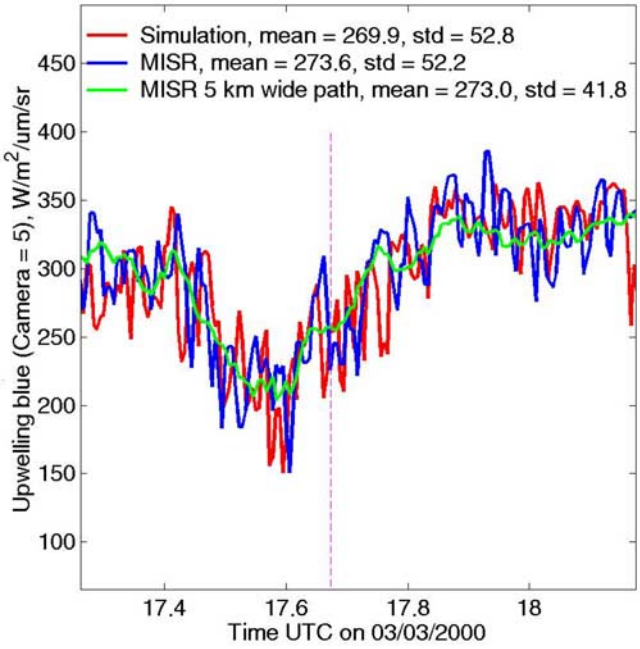

Figure 4. Comparison of MISR measurement and 2-D simulation (with additional cloud water, +0.6 K) for the MISR nadir camera at 0.446 μm. The blue line shows the MISR measurement of the closest pixel to the best guess advection path. The solid green line shows the MISR measurement of all pixels within 5 km of the advection path. Values given in the legend are for half an hour, centered on the overpass time.

range. These simulations differ only in the amount of liquid water placed in the cloud, obtained here by increasing the value of the 31.4 GHz brightness temperature used in the liquid water path retrieval (from the passive microwave radiometer). The optical depth shown in Figure 2 is based on the minimum +0.3 K solution. The increase in liquid water path from the +0.3 K solution to the +0.6 K solution is approximately 12 g/m^2, equivalent (in the case of this cloud) to an increase in the cloud optical depth of about 2.7, raising the mean optical depth from 24.3 to 27.

[13] While all three simulations require slightly increasing the brightness temperature from the measured value, these increases are all within the expected uncertainty in the measurement and underlying microwave absorption model used in retrieving the liquid water path [*Marchand et al.*, 2003]. We could have also chosen to fix the value of the cloud liquid water and alter the cloud particle size to match the solar broadband flux. However, doing this makes little difference in the final results because (1) constraining the solution to match the broadband radiometers essentially establishes the cloud optical depth and (2) there is little variation in the scattering phase function (obtained via Mie theory) associated with the required change in particle size.

[14] Figures 4 and 5 compare the MISR radiance measurements to 2-D radiative transfer simulations. Figure 4 compares the MISR nadir radiance measurement at 466 nm (blue band) along the best guess cloud advection path (solid line in Figure 1) with the simulation for this same quantity. The simulations have an apparent horizontal resolution of about 260 m, which is close to that of the MISR measurement resolution of 275 m. As the figure legend indicates, when averaged over a half-hour period centered on the overpass time, excellent agreement is observed between the simulations and measurements. However, the calculations do not match the measurements at the highest temporal/spatial frequencies (i.e., at every instant). The high-frequency structure is a result of the cloud cellular structure and, given the uncertainty in the advection path, one would not expect the simulation to exactly reproduce the measurement at these scales. That is, in Figure 4 we

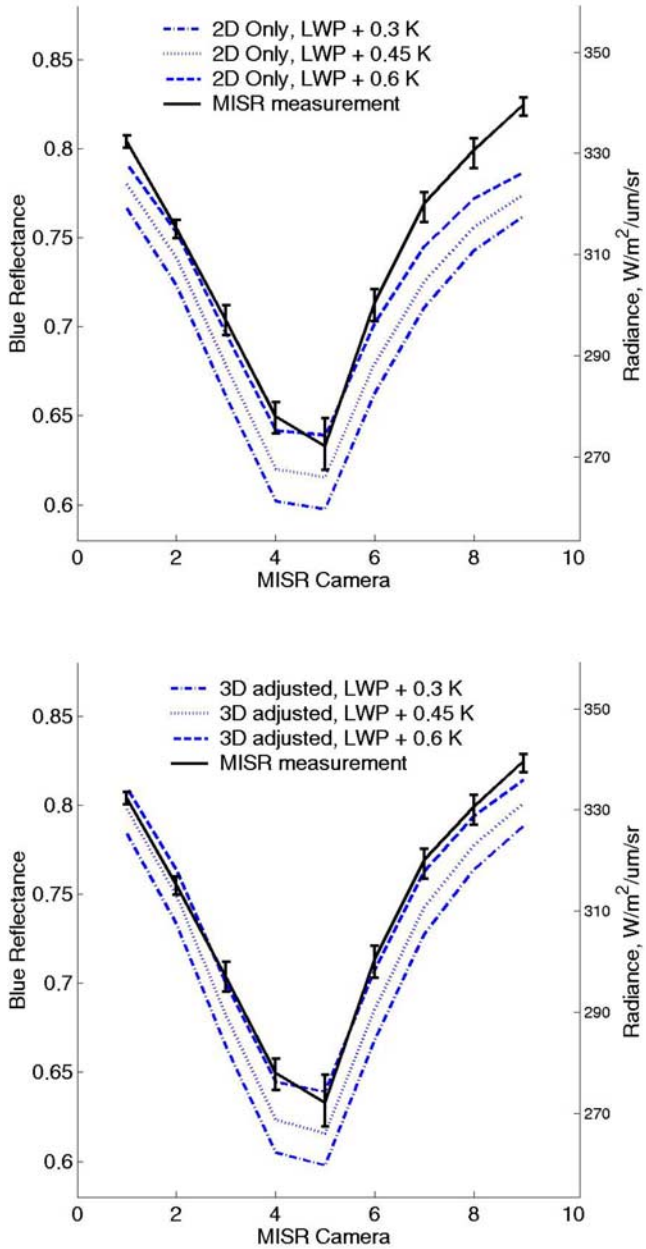

Figure 5. Comparison of mean MISR measurements to simulations for all nine MISR view angles in the MISR blue band (0.446 μm): (top) 2-D simulations and (bottom) 2-D simulation corrected for high-resolution 3-D effects as described in section 3 (for right patch).

show the result for the best guess path, but if we had chosen one of the dashed lines in Figure 1, then the measurement would have about the same average value but a different small-scale structure. We note, however, that the magnitude of the variations is similar between the simulations and MISR measurements. Part of the difference may also be a result of the cloud evolving, which is not accounted for by our advection assumption. To limit the effect of changes in the cloud structure, we restrict our analysis to a half-hour period centered on the MISR overpass time.

[15] In Figure 4 we have compared the +0.6 K simulation to the MISR measurement rather than the +0.45 K results. This was done because, as described in section 5, the +0.6 K results are more compatible with the MISR measurements at all nine observed viewing directions once 3-D effects are included in the calculations. Summary results for all three simulations, +0.3K to +0.6 K, are given in Figure 5.

[16] While the mean value of the MISR measurements and 2-D radiative transfer calculations compare very favorably at nadir, this is not the case at all of the MISR view angles. Figure 5 (top panel) shows the mean value of the MISR radiance (solid line with error bars) along the advection path over a distance equivalent to 30 min for all nine MISR view angles in the MISR blue band. As a rough measure of uncertainty in this value, the error bars show the minimum and maximum mean value obtained from MISR measurements using five different advection paths (best guess: solid line in Figure 1, plus 1 standard deviation in wind direction, minus 1 standard deviation in wind direction, plus 1 standard deviation in wind speed, and minus 1 standard deviation in wind speed).

[17] For this MISR overpass, the solar zenith angle is 45.7 degrees, and the MISR view directions are approximately 34 degrees off the solar principle plane. The MISR forward viewing cameras (1–4) observe scattering from the cloud in the forward direction (i.e., in the same direction as the incoming sunlight) and the MISR aft cameras (5–9) observe scattering back toward the Sun. The MISR view angles change slightly along the advection path (which is accounted for in the simulations) with an average view zenith angle of approximately 70.2, 60, 45.5, 25.6, 1, 26.3, 45.8, 60.3, and 70.6 degrees for cameras 1 through 9, respectively. The MISR (ellipsoid projected) radiance measurements and geometric parameters (i.e., camera view angles) are standard MISR data products freely available from the NASA Langley data archive. The results shown here are from format/version F02_0017 for the radiance data and F03_0011 for the geometric parameters. In the 2-D simulations, the simulation plane is aligned along the wind direction, which is 5° from true north.

[18] Figure 5 shows that the 2-D simulation (dashed lines) agrees well with the MISR measurements (solid lines) in most of the MISR forward viewing cameras (cameras 2–4) and at nadir (camera 5), but diverges from the simulation in the backscattering directions (cameras 6–9) and possibly in the forward most viewing direction (camera 1).

[19] If we consider only the "best" simulation with the most cloud liquid water (+0.6 K), the largest difference is only about 4%. This occurs in camera 9, which views the cloud field at a view zenith angle of 70.5 degrees. While 4% is close to the MISR project goal of 3%, the discrepancies worsen at the other wavelengths. Figure 6 (top panel) shows the relative difference between the MISR measurements and the 2-D calculations (again using the +0.6 K simulation) at all four MISR wavelengths. In this figure, the blue, green, and red curves are for the MISR blue, green, and red bands, respectively, while black is the near-infrared band. In the near-infrared, the difference exceeds 10% for camera 9. The difference between the 2-D calculations and the MISR measurements can largely be explained as a result of 3-D high-resolution cloud structure not resolved in these 2-D simulations. We will investigate the 3-D effects in sections 3 and 4, after which we adjust the 2-D results to account for 3-D effects and discuss implications for the MISR calibration in section 5.

3. Three-Dimensional Simulations

[20] With respect to the apparent difference between the baseline 2-D-only simulations and the MISR measurements with angle (see Figures 5 and 6, top panels), an analysis using 1-D radiative transfer calculations inputs (e.g., cloud particle size profile, liquid water content, various possible aerosols sizes and compositions, etc.) showed that no uncertainty in these inputs could explain this trend. Results from various published studies [e.g., *Varnai*, 2000] suggested that roughness in cloud top height might explain the difference. However, small spatial scales are not observed by the ground-based cloud radar, which we used to specify the cloud top boundary, because the radar does not make measurements sufficiently fast. In fact, because of filtering applied in the radar cloud mask algorithm [see *Clothiaux et al.*, 1995], the radar cloud top is not representative of cloud top variations at even the radar sampling rate of one observation each 10–40 s, but is smoothed at a scale equivalent to 1.5–3 km (in this case).

[21] To examine the impact of cloud top roughness and 3-D radiative transfer effects on the scattered field, we looked to AirMISR, which was flying on board the NASA ER-2 high-altitude aircraft during this experiment. AirMISR is an airborne version of the MISR instrument, but with only one camera. However, this camera can be programmed to move in flight to reproduce the MISR view angles. The AirMISR camera is of the same design as the MISR nadir camera, but because it flies much closer to the Earth, it produces smaller images with much higher spatial resolution. Figure 7 shows the AirMISR nadir near-infrared image of the cloud field captured less than 1 min after the MISR overpass.

[22] To evaluate the effect of high-resolution 3-D structure, we applied the scheme depicted in Figure 8 to obtain a 3-D description of the cloud liquid water field. In this scheme, as in the 2-D calculations in the previous section, the cloud vertical structure in terms of the profile of effective radius and the shape of the liquid water content are taken from the in situ aircraft data. The purpose of this scheme is to then estimate the column liquid water (or liquid water path) at each horizontal grid point. Once this is achieved, we can calculate the radiances at all wavelengths of interest using full 3-D radiative transfer, 1-D (i.e., independent pixel) or 2-D approaches (and at various resolutions).

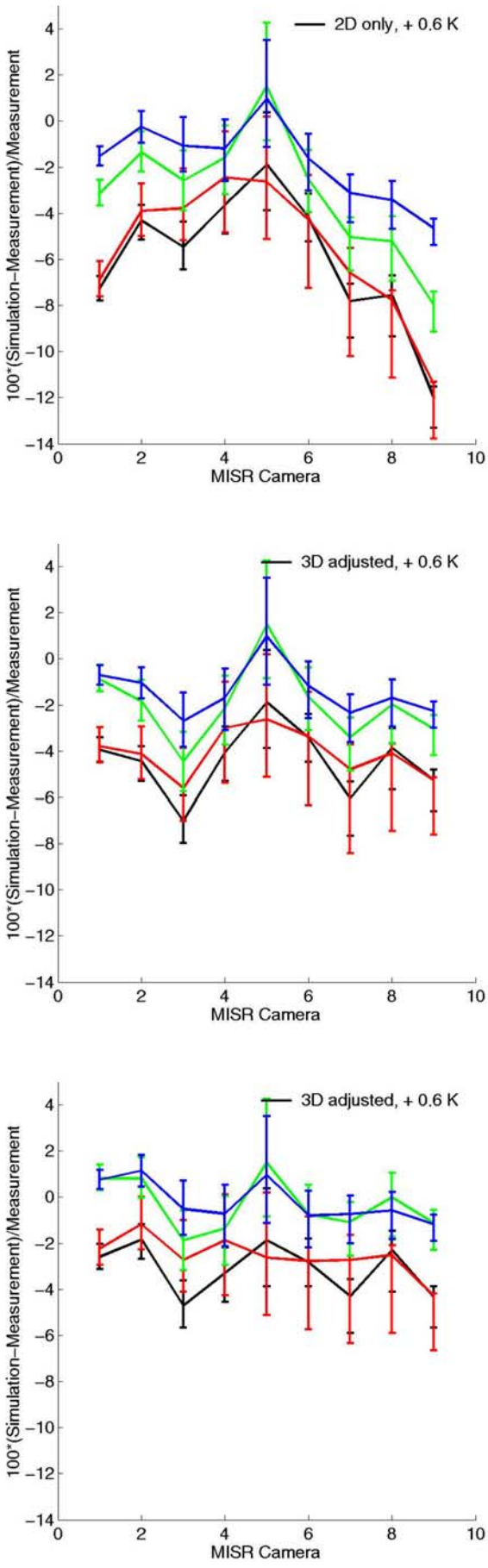

Figure 6. Relative difference between the 2-D simulations and the MISR measurements (half-hour means) in all four MISR bands: (top) without any 3-D adjustment, (middle) 3-D adjustment based on left patch (Figure 7), and (bottom) same as middle panel, only based on the right patch (see Figure 7).

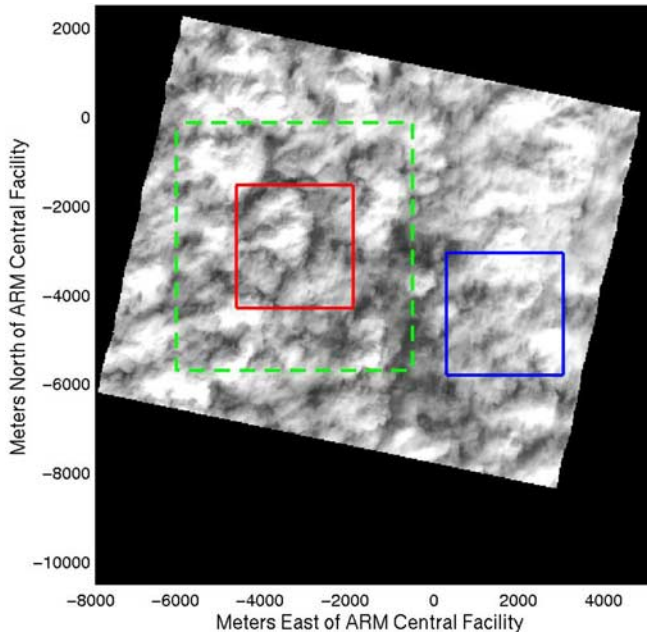

Figure 7. AirMISR view of the cloud field with 27.5 m resolution at 866 nm (near-infrared band). The boxes indicate regions of the cloud field used in the 3-D radiative transfer calculations. The 3-D calculations on the left patch (red box) were simulated using a domain restricted to only the red box and compared with calculations using the green (dashed) box. Mean values for the two calculations showed no significant differences between the two approaches, suggesting that the assumption of periodic boundary condition was satisfactory for this analysis.

[23] In our approach, we first select a subset (or patch) of the AirMISR nadir imagery. Because we have multiangle images of this same cloud scene, stereo-imaging techniques can be applied to directly determine the cloud top height. Such algorithms are currently applied to MISR data on an operational basis to determine cloud top height. Using our best guess for the cloud particle size profile and liquid water content profile (from in situ aircraft) and a fixed cloud base height (estimated from nearby lidar measurements), we estimate the liquid water path for each pixel in the AirMISR nadir scene from the measured nadir radiance at one wavelength. We opted to use the 446 nm wavelength (blue band) because the surface reflectance is small at this wavelength and because there is no significant gas absorption. This initial liquid water path estimate is based on the traditional 1-D solution. Starting with this estimate, we then use SDHOM [*Evans*, 1998] to solve the full 3-D radiative transfer problem. The solution is then compared with the measured value on a pixel by pixel basis. If the simulated nadir radiance is too large for a given pixel then the liquid water path estimate is decreased for that pixel. Similarly, if

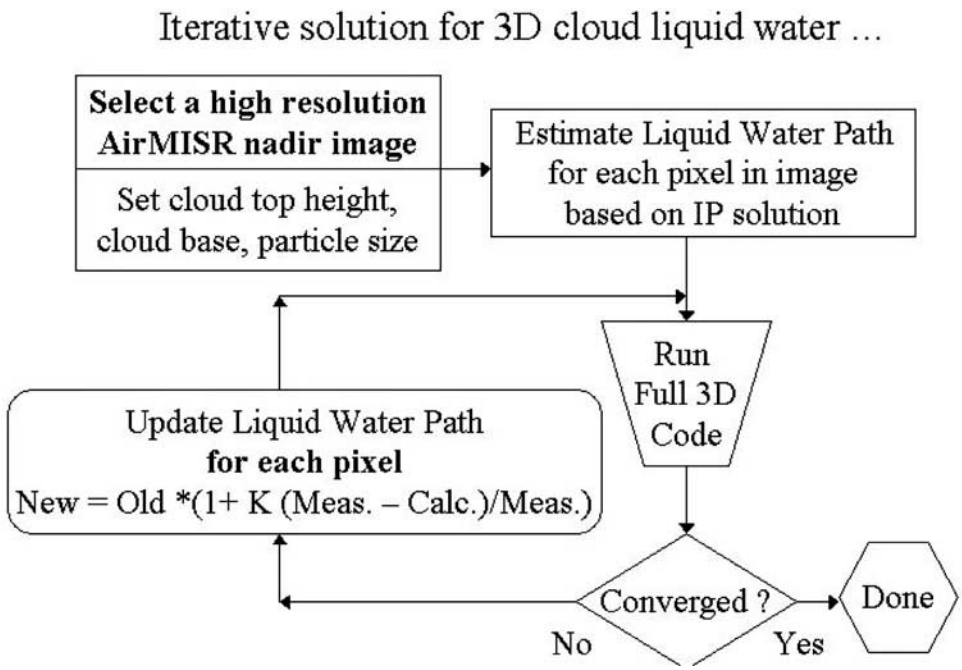

Figure 8. Scheme to obtain 3-D liquid water field. A value of $K = 1$ was found to work well.

the simulated value is too small, then the liquid water path is increased for that pixel.

[24] This process is repeated until the mean relative bias converges to better than 1%. Typically, this required only 4–10 iterations. The maximum liquid water path in any pixel was capped at 1000 g/m^2 and a few pixels did reach this level. This result occurred in places where the stereo-derived cloud top height had erred and falsely set a cloud height too low (or neighboring pixel too high), such that it was falsely shadowed by adjacent cloud elements. Because the cloud was wrongly put in a shadow, no amount of liquid water would cause the simulation to match the observed reflected sunlight. In selecting regions to simulate, we attempted to avoid these regions as much as possible but found that it was necessary to manually smooth the stereo-height field in trouble spots. We discuss this aspect and some other limitations of these calculations in more detail in Appendix A.

[25] While this approach is by no means perfect, it is largely able to capture the behavior of the mean scattered field with respect to the MISR view angles, as shown in Figure 9, for the two regions marked by solid boxes in Figure 7. In Figure 9 the solid lines are the AirMISR measurements (blue, green, red, and near-infrared bands from top to bottom) with error bars that indicate the uncertainty in aligning the same scene in all nine AirMISR camera views. While we can accurately correct for parallax between the AirMISR views, we must also compensate for the cloud advection, which is uncertain, just as the advection path of the cloud field over the ARM SGP site is uncertain. The dashed curves are the associated 3-D calculations, which were performed at 55 m (or higher) resolution.

[26] As a result of the iterative process, the measurement and simulation in the nadir (camera 5) blue band (top curve in Figure 9) are forced to agree. The agreement at all other wavelengths shows the consistency of the AirMISR measurements and the derived cloud field. The only wavelength that shows disagreement at nadir is in the AirMISR near-infrared band (solid curve near bottom of Figure 9), where the measurement is just over 5% percent brighter than the simulation. However, the surface albedo is quite bright in this band (due to surface vegetation) and the actual surface albedo at this location at the time of the MISR overpass is unknown. In the radiative transfer calculation we used a value of 0.34, which was measured at the SGP site (location 0,0 in Figure 7) using an Analog Spectral Devices spectrometer. A recently published analysis of airborne spectrometer data near the time of this MISR overpass shows considerable variation in the near-infrared albedo near the ARM SGP site [*Michalsky et al.*, 2003] and we speculate that this 5% difference is a result of the surface albedo. Otherwise, the calculations are within or very close to the estimated alignment uncertainty. It should also be mentioned that the AirMISR calibration is believe to be good to approximately 3–5%.

[27] Figure 9 also shows the radiance obtained using 2-D calculations (north-south plane) with a 275 m liquid water field and a flat cloud top (dash-dotted lines). These conditions were chosen to emulate the 2-D simulations discussed in section 2. Figure 9 shows that relative to the full 3-D calculations, the 2-D calculations noticeably underestimate the radiances in the directions observed by MISR camera 1 and cameras 7, 8, and 9 at all wavelengths. The 3-D calculations also clearly improve the agreement between the calculations and measurements in the backscattering directions, but results are mixed in the forward directions.

4. Analyis of Cloud Top Roughness and Resolution

[28] As mentioned in section 3, we can calculate the radiances from our derived three-dimensional cloud field using full 3-D, 2-D, or 1-D (i.e., independent column) radiative transfer calculations at various resolutions. To

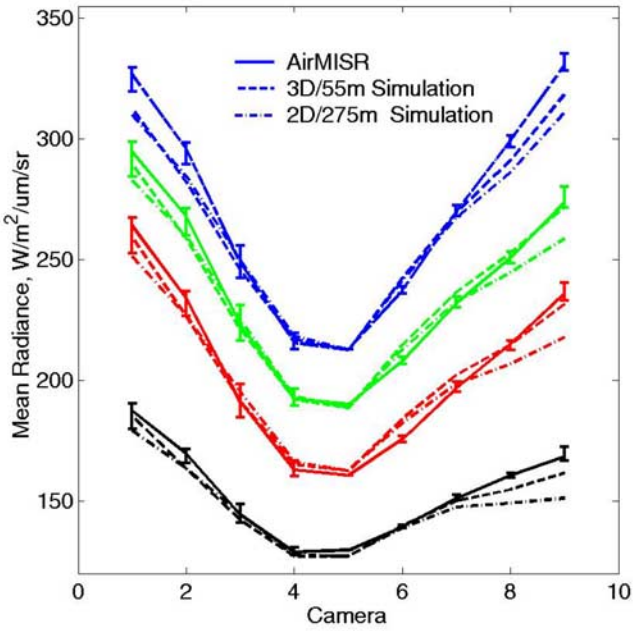

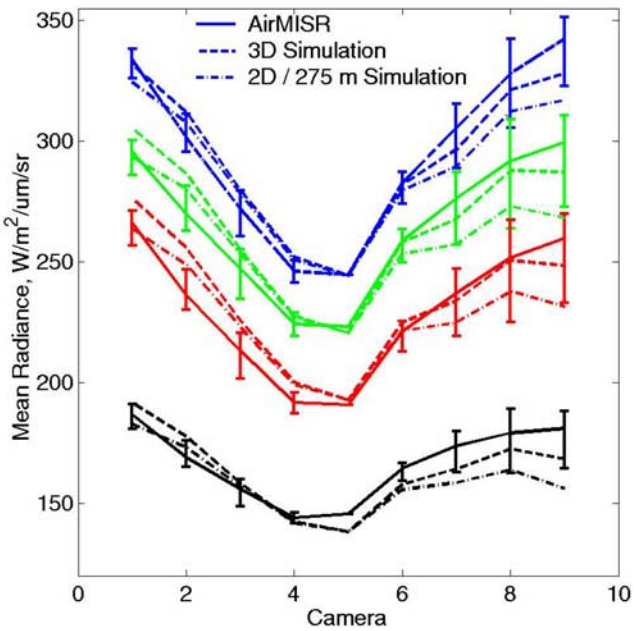

Figure 9. Comparison of AirMISR measurements (solid lines), 3-D calculations at 27.5 m or 55 m resolution (dashed lines), and 2-D calculations (dash-dotted lines) at 275 m resolution with a flat cloud top. (top) For the left patch in Figure 7. (bottom) For the right patch in Figure 7. The solid lines are the blue, green, red, and near-infrared bands from top to bottom, respectively, with error bars to indicate the uncertainty in aligning the same scene in all nine AirMISR views.

investigate the effect of changing the dimensionality and resolution, as well as to evaluate the importance of cloud top structure, we calculated the near-infrared radiances for the MISR view angles using one of our target patches. Figure 10 shows the result of these calculations for 3-D, 2-D, and 1-D radiative transfer, using 55 m and 275 m resolution. The 2-D simulations restrict variations in the cloud properties to the north-south plane, similar to those in section 2. In the case of the 275 m resolution simulations, we also ran the calculations with a fixed (or constant) cloud top height.

[29] For clarity, all of the solutions in Figure 10 have been normalized to the same value at nadir (camera 5). In reducing the resolution we simply averaged the initial liquid water field and cloud top height inputs. Because of the nonlinear relationship between cloud reflectance and liquid water path, taking the average liquid water over a region will not generally yield precisely the same mean nadir radiance as summing the contributions from a higher-resolution representation of that same region. However, the total scale change (55–275 m) is not very large and the largest adjustment for any of these solutions was only 2.5%.

[30] Comparing the highest-resolution 3-D calculations to the lower resolution 3-D calculations indicates that both higher-resolution and cloud top height structure are important at the 5% level in the backscattering directions. The increase in backscattering due to both variations in liquid water path (or cloud volume extinction) and to cloud top height variations is consistent with theoretical studies [*Varnai*, 2000]. Most theoretical studies also suggest that the forward scatter is also reduced because of shadowing. The results shown here suggest that shadowing (at least at this 45.7 degree solar zenith angle) is a weaker effect. This is consistent with recent results published by *Varnai and Marshak* [2003] down to solar zenith angles of 60 degrees.

[31] Interestingly, the 2-D calculations track the 3-D calculations quite closely in this case. This result may not

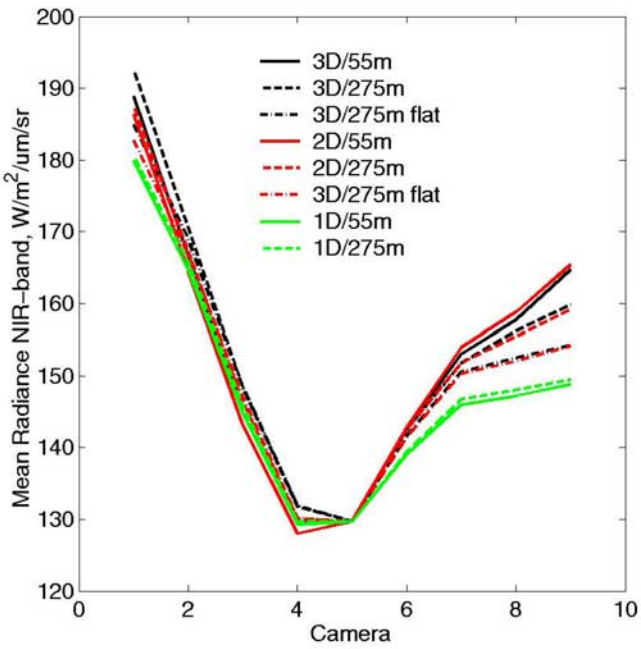

Figure 10. Comparison of simulated mean radiances for the MISR near-infrared band using 1-D, 2-D, and 3-D radiative transfer calculations at 55 m resolution, 275 m resolution, and 275 m resolution without cloud top roughness.

be robust for most inhomogeneous boundary layer clouds; other stratocumulus clouds and other solar geometries should be analyzed before drawing any general conclusions in this regard. The 1-D calculations do not account for any horizontal transport of photons or any cloud top structure. Given that the 3-D calculations show that both of these are important at the 5% level, it is not surprising to find the 1-D calculations do not perform well.

5. Adjusting 2-D Results for 3-D Effects and Implications for MISR Calibration

[32] In order to correct for 3-D and higher-spatial-resolution effects in the low-resolution 2-D calculations presented in section two (see Figures 5 and 6), we determined the multiplicative factor needed to make the 2-D calculations agree with the 3-D calculations at each wavelength and at each MISR camera view angle in Figure 9. Figure 5 (lower panel) indicates that after 3-D correction, the MISR measurements (in the blue band) are in very good agreement (better than 2%) with the +0.6 K simulation.

[33] Unfortunately, even constrained by the broadband surface flux, uncertainty in the liquid water path introduces noteworthy uncertainty in the 2-D radiance simulation. If we compare the +0.3 K simulation (the ''worst case'' simulation) with the measurements, MISR would appear to be too bright by 7% at nadir and 3.5% in cameras 1 and 9.

[34] The details of the MISR calibration are straightforward conceptually, but rather complex in practice [*Bruegge et al.*, 2002]. First an absolute calibration is applied to the nadir viewing camera in the MISR blue band. Sunlight reflected off of specially designed and carefully characterized diffuser panels (physically attached to the satellite) are then used to transfer this calibration to the other cameras (i.e., there is a diffuser-panel-based camera-to-camera or angle-relative calibration). The same panels are used to transfer the calibration from the blue band to the other MISR bands (i.e., a diffuser-based band-to-band or band-relative calibration).

[35] If one were to reduce the MISR absolute calibration (that is reduce the radiance at all angles) by 7% to force agreement between the MISR blue band measurement and the calculation at nadir for the least reflectively cloud (i.e., the worst case), then all of the MISR radiances would drop by 7%. However, this would cause MISR measurements at the most oblique view angles (cameras 1 and 9) to appear about 3.5% too low relative to the +0.3 K simulation. In other words, to make the MISR measurements at 466 nm agree with the +0.3 K simulation at 466 nm, one would have to adjust both the absolute calibration (to get the nadir value) and the camera-to-camera calibration (in a compensatory way to get agreement at the off-nadir cameras). This seems rather unlikely, and given the good agreement at all angle with the +0.6 K simulation, we conclude that the MISR absolute calibration (and angle-relative calibration) in the blue band is good to within 4%.

[36] Figure 6 (middle and lower panels) shows the remaining difference between the MISR measurements and the +0.6 simulations (after correction) for all four MISR wavelengths. The correction factors bring the MISR blue and green band data into good agreement with the simulations at all view angles. The small residual differences with angle suggest that the MISR camera-to-camera relative calibration is meeting the MISR project goal.

[37] It is encouraging that despite the obvious visible differences between our two selected patches (see Figure 7), the resulting correction is similar. For comparison, the middle panel of Figure 6 shows the 2-D simulation results after correction using the values from the right patch and the lower panel shows the 2-D simulation results after correction using the values from the left patch. This suggests that the correction is reasonably robust for this particular cloud deck.

[38] After the 3-D correction is applied to the MISR red and near-infrared bands (Figure 6, middle and lower panels, red and black lines), we again observe that the MISR camera-to-camera relative calibration appears quite good as the error is similar at all view angles. However, it is also apparent that the measurements at these wavelengths are 2–3% too bright relative to the green and blue wavelengths.

[39] In these calculations most of the scattered light reaching the MISR instrument is scattered from the cloud, where the scattering is based on appropriate Mie scattering phase functions. We expect the radiative transfer model to calculate the wavelength dependence of this scattering quite accurately. The only place in the radiative transfer calculations that exhibits notable wavelength dependence (beside the incoming solar constant) is in specifying the surface albedo. For this cloud cover, however, there is no reasonable way to increase the surface albedo sufficiently to account for the 3% excess brightness in the red band, and it requires a substantial increase in the near-infrared albedo (from 0.34 as measured at the ARM SGP site to approximately 0.5). Given the variability in the 866 nm albedo, such an increase is possible, if unlikely. However, even if the surface albedo were increased in the near-infrared, this would cause the simulation to preferentially increase the radiance in the nadir direction, and the fore and aft cameras would still appear too bright (though by less than 3%).

[40] The results of this study alone are not sufficient to consider adjusting the MISR instrument band-relative calibration. However, the MISR calibration team has conducted five other vicarious calibration experiments in which they compared MISR measurements over clear sky desert playas with AirMISR measurements and their own radiative transfer modeling. In those comparisons, they consistently found that the MISR red and near-infrared bands were too bright relative to the green and blue bands. As a result, the MISR team is currently planning to adjust the band-relative calibration coefficients so as to reduce the red and near-infrared radiances.

6. Conclusions

[41] In this study, 2-D radiative transfer calculations were compared against multiangle radiance measurements taken by the MISR instrument. Inputs to the radiative transfer calculations were derived independently from a variety of instruments, including ground-based cloud radar, wind-profiling radar, lidar, broadband solar radiometer, shadow-band radiometer (MFRSR), shortwave spectrometer, microwave radiometer, and radiosonde, as well as airborne data from AirMISR and an FSSP. Initial 2-D radiative transfer calculations compared favorably in the near nadir viewing direction and in most of the forward

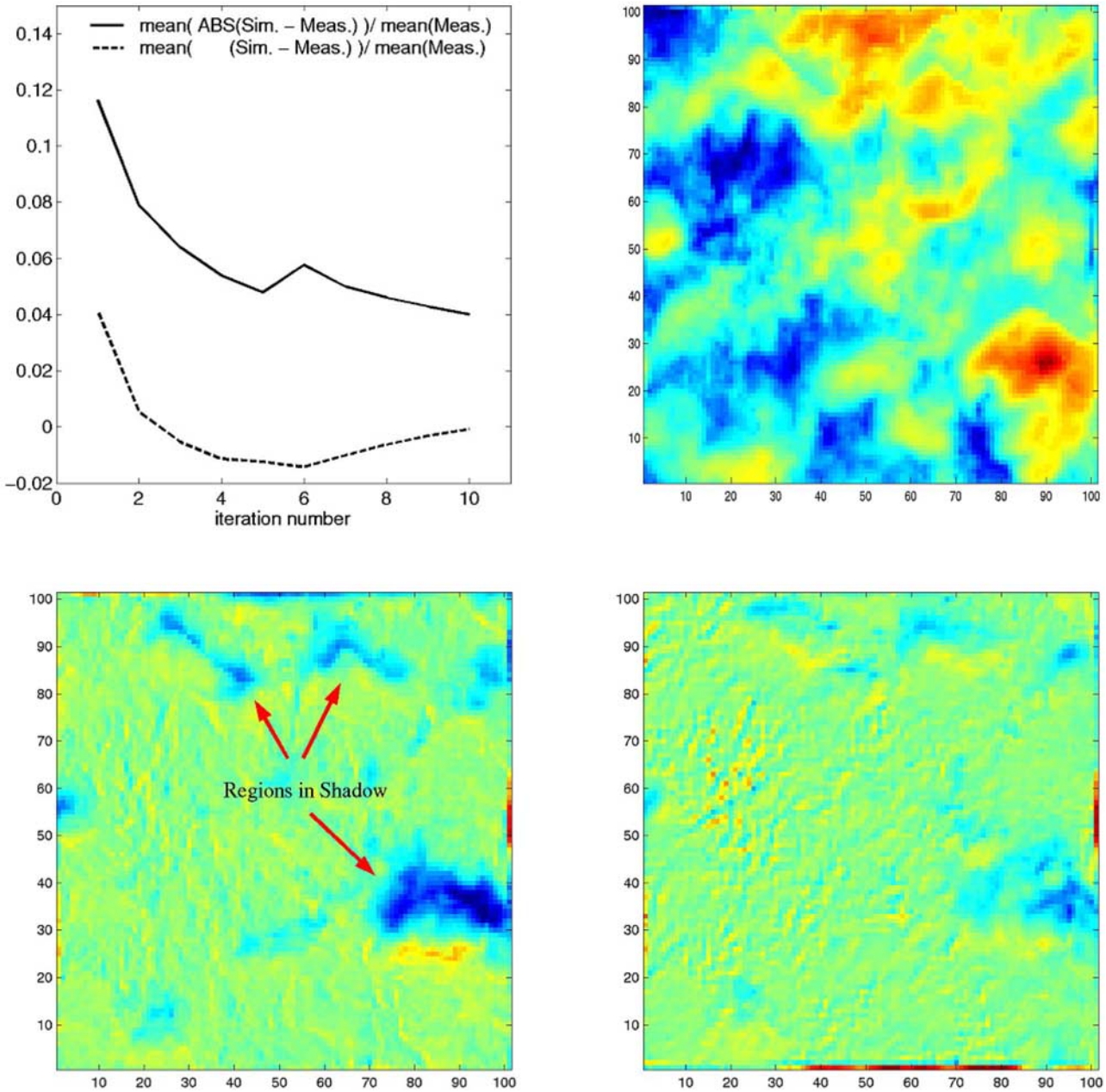

Figure A1. Comparison of AirMISR and 3-D calculations. (top left) Convergence of the simulated radiances to the AirMISR blue band measurement using the iteration scheme shown in Figure 8 for the rightmost patch shown in Figure 7. The solid line is the mean absolute deviation (normalized by the mean measured value) between the measured or input radiance imagery and the 3-D radiative transfer calculation. The dashed line is the relative bias or mean difference between the simulated image and the measurement (normalized by the mean measured value). (top right) False color image of AirMISR near-infrared measurement. (bottom right) Difference between AirMISR measurement and 3-D calculation after five iterations. (bottom left) Difference after shadow adjustment and five additional iterations.

scattering view directions, but differed by as much as 10% in the backscattering directions.

[42] Using a novel approach, 3-D radiative transfer calculations were combined with AirMISR measurements to construct a high-resolution (27.5–55 m) 3-D cloud field. Using this cloud field, it was shown that the error trends in the initial 2-D simulations were due to the 3-D structure of the cloud, including variations in cloud top height, which were not resolved in the 2-D simulations. Comparison of the 2-D calculations to the MISR measurements (after adjusting for the high-resolution 3-D structure) showed residual differences less than 4% at all angles in the MISR blue and green bands. This result suggests that the MISR absolute calibration and camera-to-camera calibration are meeting the MISR project calibration goals at these wavelengths.

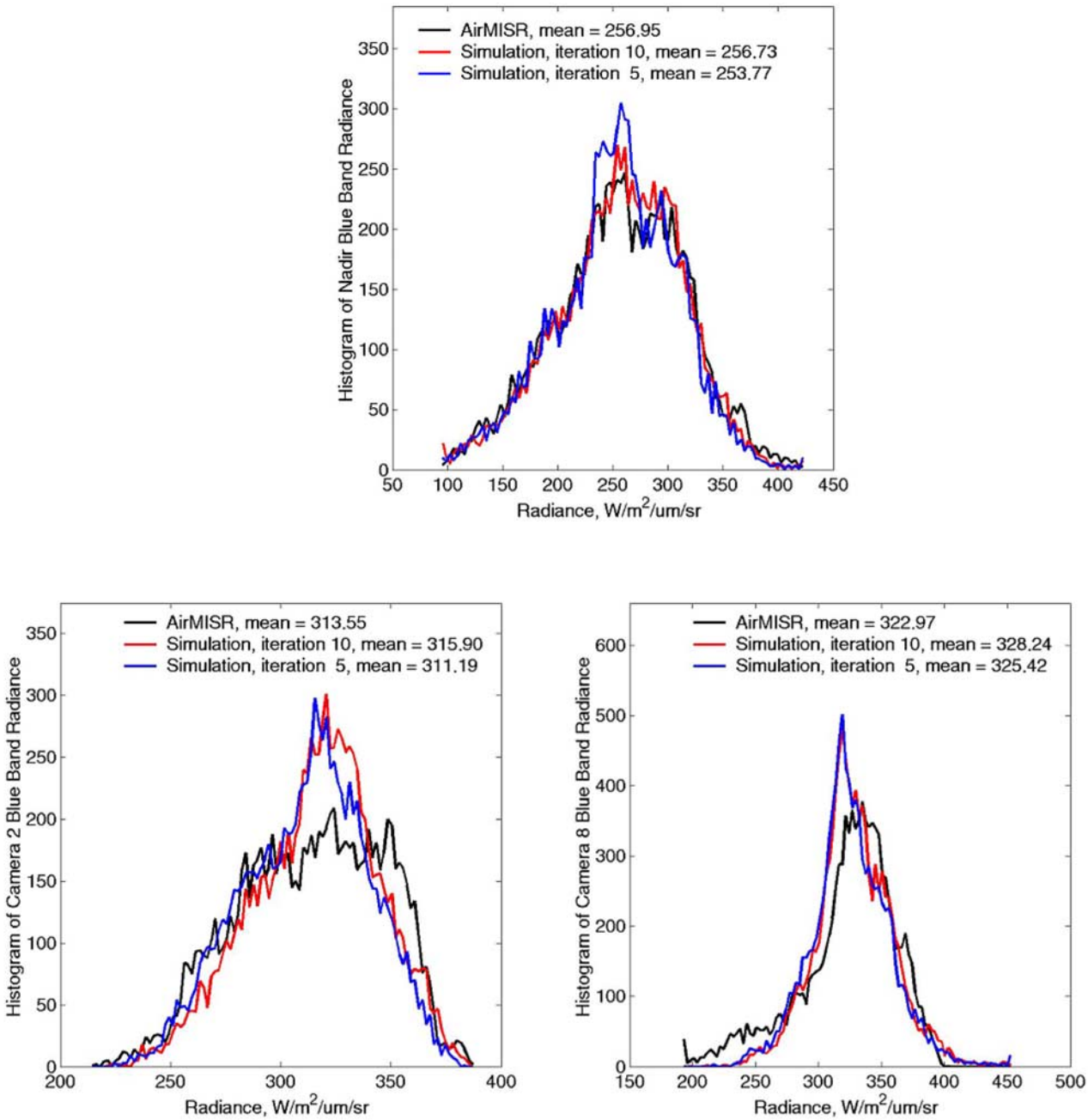

Figure A2. Histograms of the AirMISR measured radiance and 3-D calculations for three of the MISR view directions. The black line is the AirMISR measurement, the red line is the radiative transfer calculation after five iterations, and the blue line is the radiative transfer calculation after shadow adjustment and five additional iterations.

[43] The comparison also revealed that MISR measurements in the red and near-infrared bands were too bright relative to measurements in the blue and green bands. On the basis of the results of this study, along with results from five other comparisons (similar in many ways to this study but conducted over clear sky desert playas), the MISR calibration is being adjusted to reduce the red and near-infrared radiances. All MISR products regenerated since February 2004 include this correction, with MISR radiance files having a format/version number of F03_XXXX.

[44] In agreement with many previous studies [see *Varnai*, 2000], a comparison of 3-D, 2-D, and 1-D calculations for this cloud field show that variations in both cloud liquid water (or volume extinction) and cloud top height structure at scales less than 275 m are important. Widely used retrievals of cloud optical depth from visible satellite measurements are typically based on 1-D theory and are known to have problems because of unaccounted for high-resolution 3-D structure [*Iwabuchi and Hayasaka*, 2002; *Varnai and Marshak*, 2001]. The MISR measurements are clearly sensitive to these high-resolution 3-D effects, and we

believe that MISR data will prove to be of great value in learning how to correct for this structure in traditional single-view satellite retrievals.

[45] Finally, the work presented here shows that our understanding of radiative transfer in a 3-D inhomogeneous cloud has advanced such that we can model it to an accuracy of a few percent (at least when averaged on ~3-km scales). However, our ability to obtain such accuracy and perform radiative closure experiments is limited by our ability to accurately specify 3-D cloud structure. Existing measurements from the ARM program radar and microwave radiometer do not provide sufficiently accurate high-temporal-resolution data on cloud top and liquid water content variations for such purposes.

Appendix A: Additional Details on 3-D Radiative Transfer Calculations

[46] We do not claim that the iterative approach described in section 3 will work in general, only that it worked for the case examined here. While we have shown the results for only two patches, we have applied to technique to a total of five patches. All of these patches, however, do overlap the green or blue boxes in Figure 7 to some extent. Of these five patches, the right patch in Figure 7 was the most difficult, and so we concentrate on this region in this appendix.

[47] Figure A1 (top left panel) shows the convergence of the mean radiance as a function of the iteration number. Shown in this panel are the mean absolute deviation (solid line) and the relative bias (dashed line). Initially, the calculated nadir radiances were too large on average (bias near 4%), for this patch. As the iteration scheme adjusted the liquid water path in each pixel the mean absolute deviation rapidly improved, but the bias became negative. After five iterations, we examined the difference between the input radiance image and the 3-D calculated field; see Figure A1 (bottom left panel). We found that the negative bias was largely the result of several localized regions where the measured values were much larger than the simulated value. These dark regions coincided with regions which, according to the stereoscopically derived cloud top height map, should have been in shadow. After reexamining the stereo matching we found that the automated algorithm had blundered in these regions, and in fact either these pixels were too low or that neighboring pixels were too high. To correct this problem, we applied a ray tracing approach to increase the cloud top of the dark pixels just enough so that they were not shadowed.

[48] Even after correcting for these cloud top height blunders, the 3-D calculations do not perfectly reproduce the measured radiances. Figure A2 shows histograms of the radiances for the near-nadir view (input image), and a representative forward and backward view direction. In each figure we have plotted the measured results (black line) as well as the simulated values both before (blue line) and after (red line) correcting for obvious cloud top height shadowing blunders. In large measure, the simulated values cover approximately the same range of values as the measurements and the mean values (listed in the figure) compare quite favorably.

[49] In looking at all of the histograms, we noticed that as one moves away from the nadir viewing direction (in either the forward and backward scattering directions), the histograms of the calculated values appear increasingly more sharply peaked than the measured values. We speculate that this is a result of the limited angular resolution of the 3-D calculations. In these calculations we used $N_{\text{zenith}} = 16 \times N_{\text{azimuth}} = 32$ discreet ordinates. On the basis of results published by *Evans* [1998] and some of our own testing, it appears that the mean radiance is accurate to 1 or 2% in this configuration. However, 16×32 ordinates still only yields an angular resolution of approximately 10 degrees, which may smooth the radiance field making darker regions appear brighter, and brighter regions appear darker than they should be.

[50] Finally, we note that the 3-D calculations on about a 2.75×2.75 km region required one to two gigabytes of memory and pushed our SGI Origin 200 workstation very hard, requiring several days to iterate to a final solution. Thus this approach is certainly not suitable for processing satellite data on a routine basis, and will prove difficult to increase beyond 10×10 km for desktop computers at present.

[51] **Acknowledgments.** This research was supported by the MISR project, directed by David Diner, and with the assistance from the MISR calibration team led by Carol Bruegge. We would like to express our thanks to all of the MISR team, especially Mark Helmlinger, who assisted in collecting field data, and Catherine Moroney, who helped derive the stereo-based cloud top heights from the AirMISR data. We would like to give special thanks to Mike Poellet at the University of North Dakota for collecting and processing the in situ cloud measurements and to the many people in the ARM program, who collect, process, and distribute the ground-based data used in this study. Thank you.

References

Abdou, W. A., C. J. Bruegge, M. C. Helmlinger, J. E. Conel, S. H. Pilorz, W. Ledeboer, B. J. Gaitley, and K. J. Thome (2002), Vicarious calibration experiment in support of the Multi-angle Imaging Spectroradiometer, *IEEE Trans. Geosci. Remote Sens.*, *40*(7), 1500–1511.

Ackerman, T. P., D. M. Flynn, and R. T. Marchand (2003), Quantifying the magnitude of anomalous solar absorption, *J. Geophys. Res.*, *108*(D9), 4273, doi:10.1029/2002JD002674.

Baumgardner, D. (1983), An analysis and comparison of five water droplet measuring instruments, *J. Clim. Appl. Meteorol.*, *22*, 891–910.

Bruegge, C. J., N. L. Chrien, R. R. Ando, D. J. Diner, W. A. Abdou, M. C. Helmlinger, S. H. Pilorz, and K. J. Thome (2002), Early validation of the Multi-angle Imaging Spectroradiometer (MISR) radiometric scale, *IEEE Trans. Geosci. Remote Sens.*, *40*(7), 1477–1492.

Chambers, L., B. Wielicki, and N. Loeb (2001), Shortwave flux from satellite measured radiance: A theoretical study over marine boundary layer clouds, *J. Appl. Meteorol.*, *40*, 2144–2161.

Clothiaux, E. E., M. A. Miller, B. A. Albrecht, T. P. Ackerman, J. Verlinde, D. M. Babb, R. M. Peters, and W. J. Syrett (1995), An evaluation of a 94-GHz radar for remote-sensing of cloud properties, *J. Atmos. Oceanic Technol.*, *12*(2), 201–229.

Clothiaux, E. E., T. P. Ackerman, G. G. Mace, K. P. Moran, R. T. Marchand, M. A. Miller, and B. E. Martner (2000), Objective determination of cloud heights and radar reflectivities using a combination of active remote sensors at the ARM CART sites, *J. Appl. Meteorol.*, *39*, 645–665.

Davis, A. B., A. Marshak, R. F. Cahalan, and W. J. Wiscombe (1997), The Landsat scale break in stratocumulus as a three-dimensional radiative transfer effect: Implications for cloud remote sensing, *J. Atmos. Sci.*, *54*, 241–260.

Di Giuseppe, F., and A. M. Tompkins (2003), Three-dimensional radiative transfer in tropical deep convective clouds, *J. Geophys. Res.*, *108*(D23), 4741, doi:10.1029/2003JD003392.

Diner, D. J., J. C. Beckert, G. W. Bothwell, and J. I. Rodriguez (2002), Performance of the MISR instrument during its first 20 months in Earth orbit, *IEEE Trans. Geosci. Remote Sens.*, *40*(7), 1449–1466.

Dong, X. Q., P. Minnis, G. G. Mace, W. L. Smith, M. Poellot, R. T. Marchand, and A. D. Rapp (2002), Comparison of stratus cloud properties deduced from surface, GOES, and aircraft data during the March 2000 ARM cloud IOP, *J. Atmos. Sci.*, *59*, 3265–3284.

Evans, F. K. (1998), The spherical harmonics discrete ordinate method for three-dimensional atmospheric radiative transfer, *J. Atmos. Sci.*, *55*, 429–446.

Iwabuchi, H., and T. Hayasaka (2002), Effects of cloud horizontal inhomogeneity on the optical thickness retrieved from moderate-resolution satellite data, *J. Atmos. Sci.*, *59*, 2227–2242.

Loeb, N. G., and R. Davies (1996), Observational evidence of plane parallel model biases: Apparent dependence of cloud optical depth on solar zenith angle, *J. Geophys. Res.*, *101*, 1621–1634.

Marchand, R., T. Ackerman, E. R. Westwater, S. A. Clough, K. Cady-Pereira, and J. C. Liljegren (2003), An assessment of microwave absorption models and retrievals of cloud liquid water using clear-sky data, *J. Geophys. Res.*, *108*(D24), 4773, doi:10.1029/2003JD003843.

Michalsky, J., Q. Min, J. Barnard, R. Marchand, and P. Pilewskie (2003), Simultaneous spectral albedo measurements near the Atmospheric Radiation Measurement Southern Great Plains (ARM SGP) central facility, *J. Geophys. Res.*, *108*(D8), 4254, doi:10.1029/2002JD002906.

Min, Q. L., M. Duan, and R. Marchand (2003), Validation of surface retrieved cloud optical properties with in situ measurements at the Atmospheric Radiation Measurement Program (ARM) South Great Plains Site, *J. Geophys. Res.*, *108*(D17), 4547, doi:10.1029/2003JD003385.

Rahman, H., B. Pinty, and M. M. Verstraete (1993), Coupled Surface-Atmosphere Reflectance (CSAR) model: 2. Semiempirical surface model usable with NOAA Advanced Very High Resolution Radiometer data, *J. Geophys. Res.*, *98*, 20,791–20,801.

Varnai, T. (2000), Influence of three-dimensional radiative effects on the spatial distribution of shortwave cloud reflection, *J. Atmos. Sci.*, *57*, 216–229.

Varnai, T., and R. Davies (1999), Effects of cloud heterogeneities on shortwave radiation: Comparison of cloud-top variability and internal heterogeneity, *J. Atmos. Sci.*, *56*, 4206–4223.

Varnai, T., and A. Marshak (2001), Statistical analysis of the uncertainties in cloud optical depth retrievals caused by three-dimensional radiative effects, *J. Atmos. Sci.*, *58*, 1540–1548.

Varnai, T., and A. Marshak (2002), Observations of three-dimensional radiative effects that influence MODIS cloud optical thickness retrievals, *J. Atmos. Sci.*, *59*, 1607–1618.

Varnai, T., and A. Marshak (2003), A method for analyzing how various parts of clouds influence each other's brightness, *J. Geophys. Res.*, *108*(D22), 4706, doi:10.1029/2003JD003561.

Zuidema, P., and K. F. Evans (1998), On the validity of the independent pixel approximation for the boundary layer clouds observed during ASTEX, *J. Geophys. Res.*, *103*, 6059–6074.

T. Ackerman and R. Marchand, Pacific Northwest National Laboratory, P. O. Box 999, Richland, WA 99352, USA. (roj@pnl.gov)